9950-895

DRL No. 198
DRD Line Item No. SE-3

DOE/JPL-956525-83/1
Dist. Category UC-63

N84-29351

SURFACE AND ALLIED STUDIES

IN SILICON SOLAR CELLS

Quarterly
FIRST TECHNICAL REPORT
Covering period August 1983-October 1983

November 1983

by F. A. Lindholm

Contract No. 956525
University of Florida

The JPL Low Cost Solar Array Project is sponsored by the U. S. Dept. of Energy and forms a part of the Solar Photovoltaic Conversion Program to initiate a major effort toward the development of low-cost solar arrays. This work was performed for the Jet Propulsion Laboratory, California Institute of Technology by agreement between NASA and DOE.

DRL No. 198
DRD Line Item No. SE-3

DOE/JPL-956525-83/1
Dist. Category UC-63

SURFACE AND ALLIED STUDIES IN SILICON SOLAR CELLS

FIRST TECHNICAL REPORT

November 1983

by F. A. Lindholm

Contract No. 956525

The JPL Low Cost Solar Array Project is sponsored by the U. S. Dept. of Energy and forms a part of the Solar Photovoltaic Conversion Program to initiate a major effort toward the development of low-cost solar arrays. This work was performed by the Jet Propulsion Laboratory, California Institute of Technology by agreement between NASA and DOE.

TECHNICAL CONTENT STATEMENT

This report was prepared as an account of work sponsored by the United States Government. Neither the United States nor the United States Department of Energy, nor any of their employees, nor any of their contractors, sub-contractors, or their employees, makes any warranties, express or implied, or assumes any legal liability or responsibility for the accuracy, completeness or usefulness of any information, apparatus, product or process disclosed, or represents that its use would not infringe privately owned rights.

NEW TECHNOLOGY

No new technology is reportable for the period covered by this report.

TABLE OF CONTENTS

LIST OF FIGURES

ABSTRACT

Two main results are presented. The first deals with a simple method that determines the minority-carrier lifetime and the effective surface recombination velocity of the quasi-neutral base of silicon solar cells. The method requires the observation of only a single transient, and is amenable to automation for in-process monitoring in manufacturing. Distinct from many other methods in use, this method, which is called short-circuit current decay, avoids distortion in the observed transient and consequent inaccuracies that arise from the presence of mobile holes and electrons stored in the p/n junction space-charge region at the initial instant of the transient.

The second main result consists in a formulation of the relevant boundary-value problems that resembles that used in linear two-port network theory. This formulation enables comparisons to be made among various contending methods for measuring material parameters of p/n junction devices, and enables the option of putting the description in the time domain of the transient studies in the form of an infinite series, although closed-form solutions are also possible. The advantage of an infinite series formulation is the possibility of identifying dominant relaxation times of the transient, leading thereby to simplified descriptions. By outlining the derivation of open-circuit-voltage decay and junction-current recovery from this two-port formulation, we systematically compare these methods with the short-circuit-current decay method that is emphasized here. Small-signal admittance measurement methods also emerge as special cases of the two-port formulation, as is discussed briefly.

1. INTRODUCTION

Insofar as minority carriers are concerned, one may regard a solar cell as a p/n junction diode bounded by front and back surface characterized by surface recombination velocities: S_{front} and S_{back}. The surfaces may be free surfaces or internal surface, such as that adjoining the low-high junction that constitutes a back-surface field (BSF) region. This characterization places emphasis on the recombination that can take place at the surfaces, though it includes volume recombination within the cell.

For well over a decade, workers in photovoltaics have understood that the presence of a low-high junction in the BSF cell can yield an effective surface recombination velocity S_{back} on the low-doped side of the low-high junction that can be orders of magnitude below the surface recombination velocity at an ohmic contact (which is of the order of 10^6 cm/s). Accurate measurement of S_{back}, together with that of carrier lifetime in the quasi-neutral base, however, has presented problems.

More recently the importance of passivating the front surface recombination velocity to increase the power conversion efficiency has become recognized. The first recognition of this importance, by Iles, appeared in a final report (NASA 1974), of restricted distribution. The first full discussion of the importance of S_{front} in the journal literature, which emphasied experimental evidence in conjunction with a modeling of highly doped Si, by Fossum, Lindholm, and Shibib (1979), met with resistance at the outset because of the inertia of the dead-layer concept of Allison and Lindmayer (1973) of early solar-cell theory. Gradualllly an appreciation of the importance of S_{front} has emerged. One may conjecture that this emergence resulted in part from the

understanding that the huge drift field acting on minority carriers in a diffused front layer that arises in customary p/n junction theory is absent because of the dependence of the Si energy gap on the shallow-level dopant concentration.

Thus we recover the model stated in the first sentence of this INTRODUCTION: the view that a solar cell is a p/n junction bounded by front and back surface characterized by S_{front} and S_{back}. We stress the importance of experimentally determining S_{fron} and S_{back} as a function of the fabrication steps used in manufacturing.

From a theoretical viewpoint, this model yields to existing approaches for the standard solar-cell conditions: steady state (time independence) of the excitation (applied voltage or illumination). But from an experimental standpoint, steady-state excitation will not suffice for a widely applicable experimental determination of S_{front}, S_{back}, and of other parameters (such as carrier lifetime) needed for informed design. Moreover, the rapidity of measurement by transient response of these parameters makes transient measurements attractive for in-process control at key steps in manufacturing.

2. OBJECTIVES

The general purpose of this research program is to establish a methodology by which one can experimentally determine S_{front} and S_{back} and other parameters, especially carrier lifetime, of the quasi-neutral base and emitter regions. The methodology sought is to be flexible, in the sense that it will apply to a wide range of different solar-cell designs and in the sense that it will open the way to a variety of experimental techniques, thus providing cross-checks among measurements

and the interpretations springing from them. Further, we seek a methodology firmly rooted in theory, thus avoiding possible misinterpretations of data. Finally, we seek to develop experimental set-ups enabling an assessment of the utility of the methodology.

A secondary and longer-range purpose is to explore passivants of various types on the front and back surfaces.

Here we report the findings to date, both theoretical and experimental.

3. ACCOMPLISHMENTS THIS PERIOD

This report has three purposes. First, we outline a mathematical method that systematically and compactly describes the large-signal transient and small-signal frequency responses of diodes and the related devices such as transistors diodes and solar cells. This mathematical framework enables a comparison among available methods for determining carrier recombination lifetime and surface recombination velocity of quasi-neutral principal regions of the devices.

Second, exploiting this description, we survey the adequacy of various experimental large-signal transient methods for deducing these parameters. The survey is indicative, not exhaustive.

Third, we examine in detail, both theoretically and experimentally a method that apparently has not been much explored previously. We demonstrate that this method yields both the back surface recombination velocity and the recombination lifetime of the quasi-neutral base from a single transient measurement for three different $p^+/n/n^+$ back-surface-field solar cells.

4. MATHEMATICAL FRAMEWORK

In this section, we develop a mathematical framework which could be applicable to most of the large-signal transient measurement methods and could include small-signal admittance methods for the determination of the lifetime and the back surface recombination velocity of the base region of a diode or a solar cell. This analysis will treat the minority-carrier density and the minority-carrier current in a quasi-neutral base region in low injection. Focusing on the quasi-neutral base, assumed to be n-type here (of x-independent donor density N_{DD}) with no loss in generality, will simplify the treatment. Extensions to the quasi-neutral emitter are straightforward, provided one inserts the physics relevant to n+ or p+ regions.

Assume a p^+/n diode in which the uniformly doped quasi-neutral base starts at $x = 0$ and has a general contact defined by arbitrary effective surface recombination velocity S_{eff} at the far edge $x = X_{QNB}$. Such a contact could result, for example, from a back-surface-field (BSF) region. Assume also low-level injection and uniform doping of the base region. Then a linear continuity (partial differential) equation describes the excess minority holes $p(x,t)$:

$$\partial p(x,t)/\partial t = D_p \partial^2 p(x,t)/\partial x^2 - p(x,t)/\tau_p \quad , \tag{1}$$

where D_p is the diffusion coefficient and τ_p is the lifetime of holes.

If we take the Laplace transform of (1) with respect to time, we get an ordinary differential equation in x with parameter s:

$$-p(x,0^-) + sP(x,s) = D_p \, d^2P(x,s)/dx^2 - P(x,s)/\tau_p \quad , \tag{2}$$

where

$$P(x,s) = \int_{t=0}^{t=\infty} e^{-st} p(x,t)dt \quad , \quad s = \sigma + j\omega, \; j = (-1)^{1/2} \tag{3}$$

and where $p(x,0^-)$ is the initial condition for the excess hole density. Here, $t = 0^-$ denotes infitesimal negative time, and we shall treat transient excitation for which $p(x,t)$ is in the steady state for $t < 0$.

Thus $P(x) = p(x,t)$, $t<0$ where here capital P denotes a steady-state excess hole density.

Solving Eq. (2) yields

$$P(x,s) = p(x,0^-)/s + M_1 \exp(-x/L_p^*) + M_2 \exp(x/L_p^*) \tag{4}$$

where $L_p^* = (D_p \tau_p)/(1 + s\tau_p)^{1/2}$ and where M_1 and M_2, given below, are to be determined by the boundary values at the two edges of the quasi-neutral base region: $P(0,s)$ at $x=0$, and $P(X_{QNB},s)$ at $x=X_{QNB}$. Substitution of (4) into (2) yields the steady-state continuity equation for $p(x,0^-)$, verifying that (4) is the solution of (2).

Because of quasi-neutrality and low injection, the minority hole diffusion current dominates in determining the response from the quasi-neutral base. The following matrix describes the density of this current at $x = 0$ and $x = X_{QNB}$:

$$\begin{bmatrix} I(0,s) - i(0,0^-) \\ I(X_{QNB},s) - i(X_{QNB},0^-) \end{bmatrix} = \frac{eD_p}{L_p^*} \begin{bmatrix} 1 & 1 \\ e^{-X_{QNB}/L_p^*} & e^{X_{QNB}/L_p^*} \end{bmatrix} \begin{bmatrix} M_1 \\ M_2 \end{bmatrix} \tag{5}$$

where $i(0,0^-)$ and $i(X_{QNB},0^-)$ are the initial values (at $t = 0^-$) of the minority hole diffusion current at $x=0$ and $x=X_{QNB}$. In (5), hole current entering the quasi-neutral base is positive, by definition.

Regarding the minority carrier densities at the two edges as the excitation terms for a system analogous to a linear two-port network of circuit theory, we have the following two-port network matrix from (4) and (5) for the two excitations (densities) and the two responses (currents)

$$\begin{bmatrix} I(0,s) - i(0,0^-)/s \\ I(X_{QNB},s) - i(X_{QNB},0^-)/s \end{bmatrix} = \begin{bmatrix} A_{11} & A_{12} \\ A_{21} & A_{22} \end{bmatrix} \begin{bmatrix} P(0,s) - p(0,0^-)/s \\ P(X_{QNB},s) - p(X_{QNB},0^-)/s \end{bmatrix}, \quad (6)$$

where $p(0,0^-)$ and $p(X_{QNB},0^-)$ are the initial values of the excess hole densities. Equation (6) extends a similar earlier development [1] by including initial conditions so that transients may be directly studied. We call Eq. (6) the master equation for the quasi-neutral base, and the square A matrix is the characteristic matrix of the base region. In (6), $A_{12}=A_{21}= -e(D_p/L_p^*)\ \mathrm{cosech}(X_{QNB}/L_p^*)$ and and $A_{11} = A_{22} = e(D_p/L_p^*)$. Fig. 1 displays the master equation, where the initial values are included in $I(0,s)$, $-P(X_{QNB},s)$, etc. for compactness of expression.

Transient solutions can be derived from (6) by inserting proper boundary conditions, initial values and constraints imposed by the external circuit. For example, $I(0,s)=0$ in OCVD open-circuit-voltage-decay [2], $I(0,s)$=constant for reverse step recovery [3],.and $P(0,s) = 0$ for short-circuit current decay, the latter of which is developed in detail here. For small-signal methods [4]-[5], where dI, for example, is

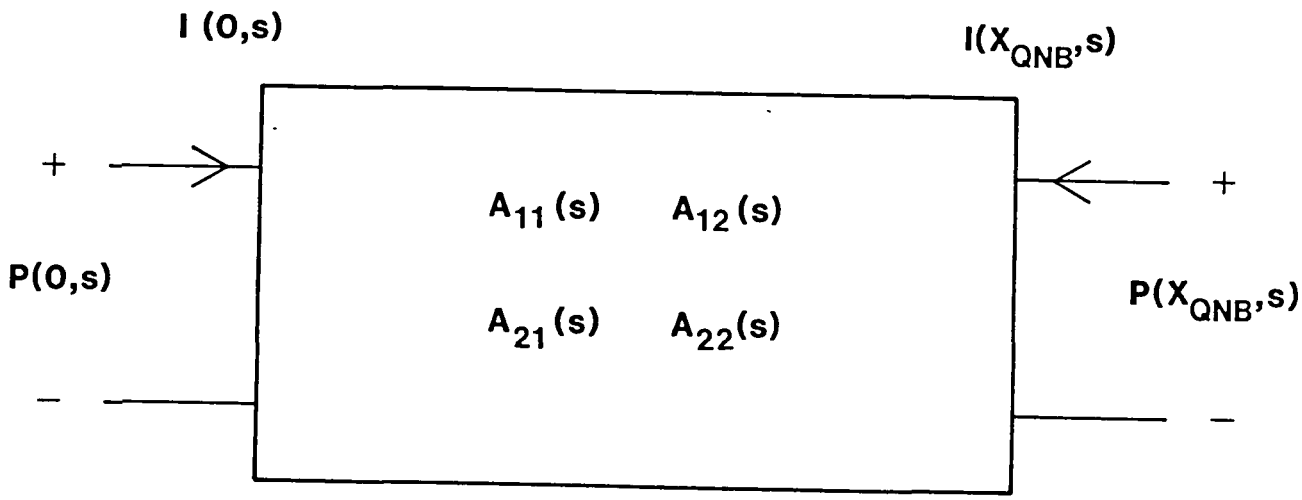

Fig. 1 Two-port network representation for hole density and hole current (density) at the two edges of the n-type quasi-neutral base region.

an incremental change of current, $I(0,s)=I_{DC}/s + dI(0,s)$ and $P(0,s)=P_{DC}/s + (edV/kT)P_{DC}$. Here the suffix DC denotes a dc steady-state variable. In later sections, we will show briefly how to get solutions from the master equation for various of these methods.

In a solar cell, the back contact system, including the low-high junction, is generally characterized in terms of effective recombination velocity, S_{eff}. The boundary condition at the back contact is $I(X_{QNB},s) = -eS_{eff}P(X_{QNB},s)$. From a circuit viewpoint, this relation is equivalent to terminating Fig. 1 by a resistor of appropriate value dependent partly on S_{eff}. Because S_{eff} in part determines the transient in the various methods named above, we can determine S_{eff} from the transient response, as will be shown.

In Secs. 6 to 8 we consider the utility of the master equation in characterizing selected measurement methods. The main emphasis will be placed on the short-circuit current decay (Sec. 8).

Before doing this, however, we shall remark on the simplicity provided by the master equation (Eq. 6) by comparing it with its counterpart in the steady state.

5. TRANSIENT VS. STEADY-STATE ANALYSIS VIA TWO-PORT TECHNIQUES

In general, the current (current density for a unit area) is the sum of the hole current, the electron current and the displacement current. For the quasi-neutral regions under study using the two-port technique described in Sec. 4, the displacement current is negligible. In the steady state, the two-port description leading to the master equation simplifies because then the hole current in our example of Sec. 4 depends only on position x. This x-dependence results from

volume recombination (relating to the minority-carrier lifetime) and effective surface recombination (relating to the effective surface recombination velocity). A two-port formulation for the steady state leads to the same matrix description as that derived previously, in which the matrix elements $A_{ij}(s)$ of Eq. (6) still hold but with the simplification that $s = 0$. From such a master equation, one can determine the hole current at the two edges of the quasi-neutral base; and, using quasi-neutrality together with knowledge of the steady-state currents in the junction space-charge region and in the p^+ quasi-neutral emitter region, one can thus find the steady-state current flowing in the external circuit or the voltage at the terminals of the diode. If the quasi-neutral base is the principal region of the device, in the sense that it contributes dominantly to the current or voltage at the diode terminals, then one has no need to consider the current components from the other two regions.

In contrast the general time-varying mode of operation leads to a minority hole current in the n-type quasi-neutral base of our example that depends on two independent variables, x and t. The time dependence results because the holes not only recombine within the region and at its surface, but also their number stored within the base varies with time. This may be regarded as resulting from the charging or discharging hole current associated with $\partial p/\partial t$ in the hole continuity equation. This charging or discharging current complicates the variation of the hole current in space and time. But the use of the Laplace transform of the two-port technique in effect reduces the complexity of the differential equation to the level of that describing the steady state; the dependence on variable t vanishes, reducing the

partial differential equation to an ordinary differential equation in x, just as in the steady state.

This comparison also brings out another point. Just as in the steady state, one must interpret the transient voltage and current at the diode terminals as resulting not only from the quasi-neutral base but also from the junction space-charge region and the quasi-neutral emitter. In the interpretation of experiments to follow, we shall discuss complications arising from this multi-regional dependence.

6. OPEN CIRCUIT VOLTAGE DECAY (OCVD)

In this widely used method [2], the free carriers in the junction space-charge region enter to contribute to the transient. But, consistently with Sec. 4, and with most common usage, we concentrate at first on the n-type quasi-neutral base.

From the master equation [Eq. (6)], the transient solution for the junction voltage is obtained from open-circuit constraint (for $t > 0$) that $I(0,s)=0$:

$$P(0,s) = p(0,0^-)/s - \frac{i(0,0^-)L_p^*}{eD_p s} \quad \frac{1 + \{D_p[\coth(X_{QNB}/L_p^*)]/L_p^* S_{eff}\}}{\coth(X_{QNB}/L_p^*) + (D_p/L_p^* S_{eff})} \quad . \tag{7}$$

Here we have assumed that the quasi-neutral base is the principal region in the sense described in Sec. 4; that is, we neglect contributions from all the other regions of the device.

Using the Cauchy's residue theorem, we find the inverse transform of Eq. (7):

$$p(0,t) = -\sum_{i=1}^{\infty} \frac{2i(0,0^-)L_p}{eD_p s_i \tau_p} \frac{[1 + (D_p K_i/L_p S_{eff})\cot(X_{QNB}K_i/L_p)]\exp(s_i t)}{[(X_{QNB}/L_p)\mathrm{cosec}^2(X_{QNB}K_i/L_p) + (D_p/L_p S_{eff})]}$$

(8)

where s_i is the ith singularity point (ith mode) which satisfies the Eigenvalue equation,

$$\coth(X_{QNB}\sqrt{1+s_i\tau_p}/L_p) + D_p\sqrt{1+s_i\tau_p}/L_p S_{eff} = 0 \qquad (9)$$

and $K_i = \sqrt{-1-s_i\tau_p} > 0$, where $s_i < 0$.

As can be seen in Eq. (8), the decay of the excess hole density at x=0 is a sum of exponentials; each Eigenvalue s_i is called a mode, as in the electromagnetic theory. Appendix A treats the details of determining the Eigenvalues s_i from Eq. (9) (and from the similar Eq. (11) derived below).

The decaying time constant $-1/s_1$, of the first mode is much the largest of the modes. Both s_1 and the initial amplitude of the first mode are functions of S_{eff} and τ_p. Thus separating the first mode from the observed junction voltage decay curve, by identifying the linear portion of v(t), will enable, in principle, determination of S_{eff} and τ_p simultaneously. But our recent experience, coupled with that cited in [6], suggests that this is seldom possible in practice for Si devices at $T \simeq 300$ K. In Si devices the open-voltage decay curve is usually bent up or bent down because of discharging and recombination within the space-charge region.

As mentioned in [4], the mobile charge within the space-charge region contributes significantly to the observed voltage transient for

Si, in which $n_i \sim 10^{10}$ cm^{-3}, but not in Ge, for which OCVD was first developed, and for which $n_i \sim 10^{13}$ cm^{-3}. Here n_i is the intrinsic density and is also the ratio of the pre-exponential factors that govern contributions from the quasi-neutral regions relative to those from the junction space-charge region.

Thus we identify the transient decay of mobile electrons and holes within the p/n junction space-charge region, which persists throughout the open-circuit voltage decay (OCVD), as a mechanism that distors OCVD so significantly that the conventional treatment of OCVD will not reliably determine τ_p or S_{EFF}. The conventional treatment is consistent with that proceeding from the master equation, as described in this section. The interested reader may consult Ref. 4 for experimental comparisons that lead to this conclusion. We shall not pause here to present these.

Rather we shall turn briefly to possible methods to remove the effects of this distortion. In an attempt to characterize the space-charge-region contribution to the observed transient voltage [6], quasi-static approximations and a description of the forward-voltage capacitance of the space-charge region based on the depletion approximation were combined to give rough estimates of this contribution. We plan to refine the approximations and the estimates in a future publication, leading possibly to a variant of OCVD useful for determining τ_p and S_{eff}.

7. REVERSE STEP RECOVERY (RSR)

For this method [3], in which again the diode is subjected to steady forward boltage for $t > 0$, we have two constraints (for $t > 0$).

The first is $I(0,s)$ = constant (reverse current), $0 < t < \tau_s$, where τ_s is the time needed for the excess hole density $p(0,t)$ to vanish. This is the primary constraint. (The second constraint is $p(0,t) \simeq -n_i^2/N_{DD}$ for $\tau_s < t < \infty$, a result of applied reverse bias through a resistor.)

The primarily observable storage time τ_s is estimated by following a procedure similar to that described in Sec. 4, proceeding from the master equation.

This method suffers difficulties similar to that of the OCVD method. Because $p(0,t) > 0$ for $0 < t \leq \tau_s$, the decay of mobile hole and electron concentrations in the p/n junction space-charge region complicates the interpretation of the measured τ_s in terms of the desired parameters, τ_p and S_{eff}.

In addition to this, during the portion of recovery transient occuring for $\tau_s < t < \infty$, the reverse generation current is often large enough to saturate the recovery current so quickly that we have no sizable linear portion of the first-mode curve on a plot of $\ln[i(t)]$ vs. t. This linear portion provides interpretable data for Ge devices [3], but not often for Si devices according to our experiments.

We shall not pause here to present experimental evidence, but rather postpone that presentation until a planned fuutre publication where comparison with previous work can be comprehensive.

8. SHORT CIRCUITED CURRENT DECAY (SCCD)

8.1 Brief Physics and Mathematics

In this method, one first applies a forward bias to set up a steady-state condition and then suddenly applies zero bias through a resistance so small that the constraint is essentially that of a short

circuit. Thus, for $t > 0$, the p/n junction space-charge and quasi-neutral regions discharge. One measures the transient current via the voltage across the small resistor. If the discharging time constants related to the charge stored within the quasi-neutral emitter and the junction space-charge region are much smaller than from the quasi-neutral base, one can separate the first mode of the quasi-neutral-base response and determine S_{eff} and τ_p.

We first consider the time of response of the junction space-charge region. Upon the removal of the forward voltage, the constraint at the terminals becomes essentially that of a short circuit. The majority-carrier quasi-Fermi levels at the two ohmic contacts immediately become coincident, and the junction barrier voltage rises to its height at equilibrium within the order of the dielectric relaxation time of the quasi-neutral regions, times that are of the order of no greater than 10^{-12}s. This occurs because the negative change in the applied forward voltage introduces a deficit of majority holes near the ohmic contact of the p^+ emitter and a deficit of majority electrons near the ohmic contact in the quasi-neutral base. The resulting Coulomb forces cause majority carriers to rush from the edges of the junction barrier regions, thus causing the nearly sudden rise of the barrier height to its equilibrium value. (The physics governing this phenomena comes from Maxwell's Curl $\underline{H} = \underline{i} + \partial\underline{D}/\partial t$; taking the divergence of both sides yields $0 = \text{div}\ \underline{i} + \partial(\text{div}\ \underline{D})/dt$, which, when combined with $\underline{i} = (\sigma\underline{D}/\varepsilon)$ and $\text{div}\underline{D} = \rho$, yields a response of the order of ε/σ, the dielectric relaxation time.)

Following this readjustment of the barrier height, the excess holes and electrons exit the junction space-charge region within a transit

time of this region (about 10^{-11}s typically), where they become majority carriers in the quasi-neutral region and thus exit the device within the order of a dielectric relaxation time.

Thus the discharging of excess holes and electrons within the junction space-charge region in the SCCD method occurs within a time of the order of 10^{-11}s, which is much less than any of the times associated with discharge of the quasi-neutral regions. This absence in effect of excess holes and electrons within the junction space-charge region greatly simplifies the interpretation of the observed transient. It is one of the main advantages of this method of measurement.

A more detailed discussion of the vanishing of excess holes and electrons within the junction space-charge region appears in Appendix B.

The discharge of the quasi-neutral emitter depends on the energy-gap narrowing, the minority carrier mobility and diffusivity, the minority-carrier lifetime, and the effective surface recombination velocity of this region. For many solar cells, this discharge time will be much faster than that of the quasi-neutral base, and we shall assume this is so in the discussion to follow.

Having established that the mobile carriers in the junction space-charge region enter the short-circuit-decay transient during an interval of time too short to be observed, and noting also now that negligible generation or recombination of electrons or holes within this region will occur during the transient, we now turn to the observable transient current. Inserting the constraint, $P(0,s) = 0$, into the master equation, Eq. 6, leads to

$$I(0,s) = i(0,0^-)/s - \frac{eD_p p(0,0^-)}{sL_p^*} \frac{\coth(X_{QNB}/L_p^*) + D_p/L_p^* S_{eff}}{1 + [D_p/L_p^* S_{eff}]\coth(X_{QNB}/L_p^*)} \quad . \tag{10}$$

Cauchy's residue theorem yields the inverse transform of (10):

$$i(t) = -\sum_{i=1}^{\infty} \frac{eD_p p(0,0^-)K_i}{s_i L_p} \frac{\cot(K_i X_{QNB}/L_p) - D_p K_i/L_p S_{eff}}{(\tau_p/2K_i^2) + (X_{QNB}/2S_{eff})\mathrm{cosec}^2(K_i X_{QNB}/L_p)} e^{s_i t} \quad , \tag{11}$$

where s_i is the ith singularity which satisfies the Eigenvalue equation,

$$1 + \frac{D_p}{L_p S_{eff}} \sqrt{1+s_i\tau_p}\, \coth\left[\frac{X_{QNB}}{L_p}\sqrt{1+s_i\tau_p}\right] = 0 \quad , \tag{12}$$

and where $K_i = (-1-s_i\tau_p)^{1/2} > 0$, with $s_i < 0$.

Truncating (11) and (12) to include only the first mode s_1, we obtain from (11) and (12):

$$1 + (D_p/L_p S_{eff})\sqrt{1 + s_1\tau_p}\, \coth[(X_{QNB}/L_p)(1 + s_1\tau_p)^{1/2}] = 0 \tag{13}$$

and

$$i_{\text{first mode}}(0) =$$

$$-\frac{eD_p p(0,0^-)K_1}{s_1 L_p} \frac{\cot(K_1 X_{QNB}/L_p) - (D_p K_1/L_p S_{eff})}{(\tau_p/2K_1^2) + (X_{QNB}/2S_{eff})[\mathrm{cosec}^2(K_1 X_{QNB}/L_p)]} \quad . \tag{14}$$

Equations (13) and (14) contain four unknowns: $i_{first\ mode}(0)$, s_1, τ_p and S_{eff}. The parameters, s_1 and $i_{first\ mode\ (0)}$ are determined from the staight-line portion of the observed decay (in Fig. 3c to be discussed below): $p(0,0^-) = (n_i^2/N_{DD})[\exp(ev(0^-)/kT)-1]$. Here $v(0^-)$ is known from the steady forward voltage applied for $t < 0$ and the doping concentration N_{DD} of the base is measured by usual methods; $D_p(N_{DD})$ is known from the standard tables and X_{QNB} is measured. Combining (14) and (13) then yields the desired parameters: τ_p and S_{eff}.

8.2 Experiments and Results

To explore the utility of the SCCD method, we connect the solar cell under study to node B of the electronic switching circuit illustrated in Fig. 2.

The circuit works as follows. When $V_1(t)$ is high, switching transistor T_1 turns on, which charges the large capacitor in parallel with it and divides the high voltage V_A about equally between the solar cell and the emitter-collector terminals of the transistor. Thus the voltage across the solar cell becomes about 0.6 V, which one may control by altering $(V_1)_{high}$, the variable resistor connected to the transistor base, or both. In this mode, the quasi-neutral base charges to store ultimately a steady-state charge of excess holes and electrons, and $p(0,0^-)$ of Eqs. (10), (11) and (14) is established.

Now assume that V_1 drops to its low value, an incremental change of about 0.6 V. The capacitor across the transistor acts as an incremental short circuit and the voltage across the solar cell suddenly vanishes to a good approximation, thereby establishing the desired short-circuit constraint. The large capacitor maintains this constraint nearly

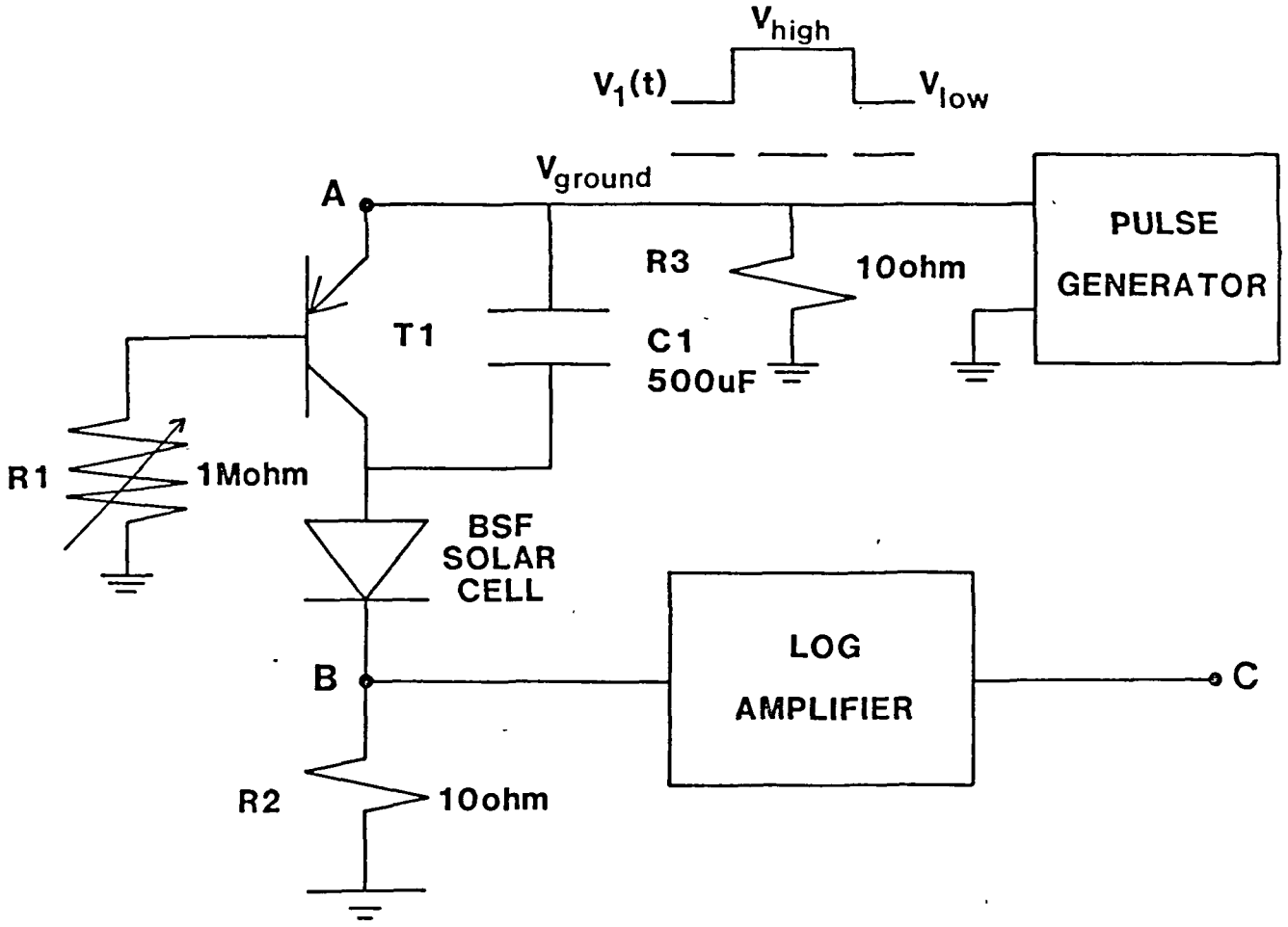

Fig. 2 The electronic switching circuit used in the SCCD method. The circuit elements are: switching transistor is 2N3906, the pulse generator is HP 8004, and the logarithmic amplifier consists of the usual configuration of an operational amplifier (Burr-Brown 3500C) connected to node B through a 100 ohm resistor and across which (between nodes B and C) two oppositely directed switching diodes (IN914) constitute the feedback loop.

perfectly during the first-mode transient of the solar cell; that is, during this transient, this capacitor and the input voltage source, which has a small resistance of 50 Ω (in parallel with 10 Ω), act as nearly incremental short circuits. Thus the desired short-circuit constraint is maintained to a good approximation during the SCCD transient of interest.

We used three different $p^+/n/n^+$ BSF solar cells for which the parameters are: DEVICE 1--N_{DD} (substrate doping) = 6×10^{14} atoms/cm^3; X_{QNB} (base thickness) = 348 μm, area = 4 cm^2; DEVICE 2--N_{DD} = 7×10^{14} atoms/cm^3, X_{QNB} = 320 μm, area = .86 cm^2, DEVICE 3--N_{DD} = 3.5×10^{15} atoms/cm^3, X_{QNB} = 348 μm, area = 4 cm^2.

We measured the voltage across the solar cell under study. As illustrated in Fig. 3(a), the voltage drops by 0.1 V within 1 μs. This means that the excess minority carrier density p(0,t) drops to 2% of its initial value within 1 μs. The speed is circuit limited. One could design a much faster circuit. Here $\tau_d = -1/s_1$ is the first-mode decay time, influenced by both volume and surface recombination in the base. But the circuit used suffices because $\tau_p \gg 1$ μs for the solar cells studied. Fig. 3(b) shows the current during the transient. Fig. 3(c) is its semi-logarithmic counterpart, illustrating the straight-line position of the transient obtained from the output of the logarithmic amplifier in Fig. 2. From this τ_d is determined. Since the voltage at node B is purely exponential for a time, the corresponding output voltage at node C is linear in time, as Fig. 3(c) illustrates. We used switching diodes in the log amplifier whose I-V characteristic is $V = .0385 \ln(I/I_o+1)$. If the first-mode current is

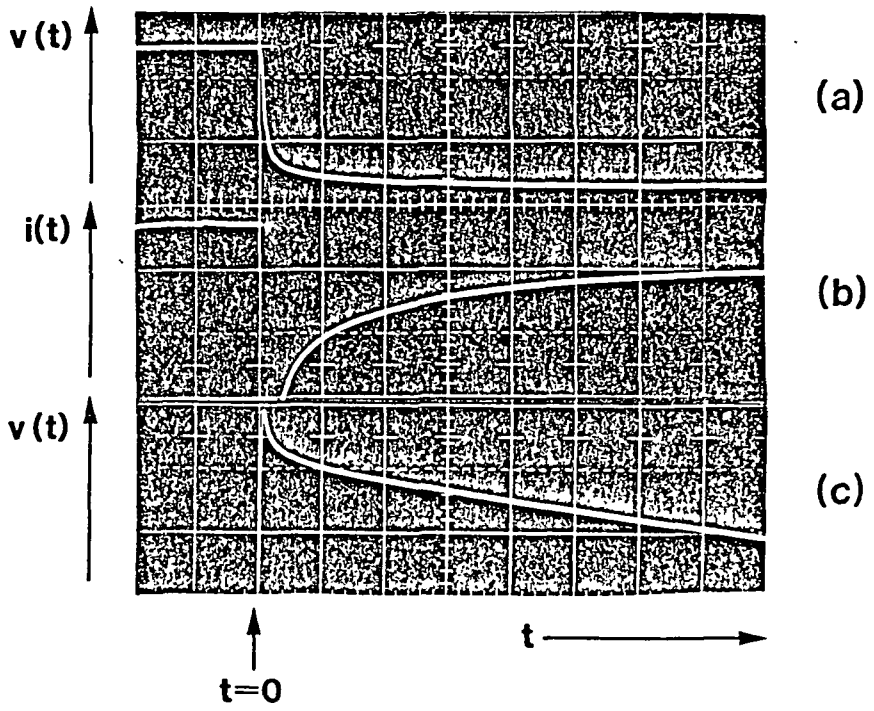

Fig. 3 (a) Voltage across BSF #1 solar cell (vertical:.2V/div).
(b) Current through BSF #1 solar cell (vertical:1mA/div).
(c) Log scale representation of (b) (vertical:.1V/div), where $v(t) = (mkT/e)\log_e[i(t)/I_o + 1]$.
In (a)-(c), horizontal axis is 10 μs/div.

$$I_{\text{first-mode}}(t) = \text{constant } \exp(-t/\tau_d) \quad , \quad \tau_d \tilde{=} -1/s_1 \quad , \tag{15}$$

then the slope of the output voltage of log amplifier is $-38.5\ \text{mV}/\tau_d$. Extrapolation of the straight portion in Fig. 3(c) yields the initial value of $i_{\text{first-mode}}(0^+)$ as the intercept.

We measured the decay time constant and the initial amplitude of the first-mode current as follows. For DEVICE 1, $\tau_d \equiv -1/s_1 =$ 29.3 μsec, $i_{\text{first-mode}}(0^+) = 2.73$ mA for $v(0^-) = 0.44$ V and T = 303.1 K. For DEVICE 2, $\tau_d = 24.5$ μsec, $i_{\text{first-mode}}(0^+) = 4.35$ mA for $v(0^-) = 0.5$ V and T = 302.9 K. For DEVICE 3, $\tau_d = 28.5$ μsec, $i_{\text{first-mode}}(0^+) =$ .696 mA at $v(0^-) = .47$ V and 303.5 K. Here $v(0^-)$ denotes the steady forward voltage applied across the solar cell before transient.

From the above development, these results give: For DEVICE 1, $\tau_p =$ 119 μs, $S_{eff} = 25$ cm/s; for DEVICE 2 = $\tau_p = 119$ μs, $S_{eff} = 60$ cm/s; for DEVICE 3, $\tau_p = 213$ μs, $S_{eff} = 100$ cm/s. These results agree favorably with those obtained for the same devices by using the more time-consuming methods detailed in [4] - [5].

9. DISCUSSION

Most measurement methods for the determination of the minority-carrier lifetime and the surface recombination velocity of the base region of Si solar cells share a common problem caused by the existence of the sizable number of the mobile carriers within the space-charge-region. These methods, among open-circuit voltage decay (Sec. 6) and reverse step recovery (Sec. 7), were originally developed for Ge devices. Si has a much larger energy gap E_G than does Ge. Thus the

distortion of the measured response by carriers stored in the junction space-charge region is much more pronounced in Si, mathematically because of the role of the intrinsic density n_i discussed in Sec. 6.

If the electronic switch providing the short circuit closes fast enough, the mobile holes and electrons stored for negative time in the junction space-charge region play no role in determining the response of the short-circuit-current decay described in Sec. 8. In our experiments, the simple circuit of Fig. 2 had speed limitations, but these limitations did not markedly influence the accuracy of the determined base lifetime and surface recombination velocity. This lack of influence results because the decay time of the first-mode response, which accounts for vanishing of minority holes both by volume recombination within the quasi-neutral base and effectively by surface recombination, greatly exceeded the time required for the excess hole density at the base edge of the space-charge region to decrease by two orders of magnitude. Details concerning this issue appear in Sec. 8.

Apart from this potential circuit limitation, which one can overcome by improved circuit design, a more basic consideration can limit the accuracy of the short-circuit-current decay (SCCD) method. In general, the current response derives from vanishing of minority carriers not only in the quasi-neutral base but also in the quasi-neutral emitter. For the solar cells explored in this study, the emitter contributes negligibly to the observed response because of the low doping concentration of the base and because of the low-injection conditions for which the response was measured. But for other solar cells or for higher levels of excitation, the recombination current of the quasi-neutral emitter can contribute significantly.

The contribution from the quasi-neutral emitter may be viewed as an opportunity rather than as a limitation. That is, the SCCD method may have utility wider than that treated here. If the quasi-neutral emitter contains excess charge whose decay time dominates in determining the transient observed, in some devices the parameters of the physical electronics of the highly doped and thin quasi-neutral emitter can be explored using SCCD. An example may be a transistor with a thin and highly doped base region or a solar cell having a high open-circuit voltage controlled by the recombination current in the emitter. For such devices, the absence of contributions from carriers in the junction space-charge region becomes a particularly key advantage not offered by either open-circuit voltage decay or step reverse recovery. The SCCD method also may enable parameter determination if high injection in the base prevails. Exploring these possible uses will require fast switching circuits and determination of the existence of a dominant relaxation time from minority carriers in the highly doped emitter.

Note that the SCCD method determines the base lifetime and the effective surface recombination velocity of a BSF solar cell by a single transient measurement. One can easily automate the determination of these parameters from parameters directly measured from the transient by a computer program, and the measurement itself may be automated. This suggests that SCCD may be useful for in-process control in solar-cell manufacturing.

This paper began with a mathematical formulation of the relevant boundary-value problem that led to a description similar to that of two-port network theory. The advantages of this formulation were only touched upon in Sec. 3 and only the bare elements of its relation to

open-circuit voltage decay and step reverse recovery were developed. Further exploitation to enable systematic development and comparison of small-signal and transient methods for the determination of material parameters of solar cells and other junction devices is planned as a subject for future study.

REFERENCES

1. F. A. Lindholm and D. J. Hamilton, "A systematic modeling theory for solid-state devices", Solid-State Electron., vol. 7, pp. 771-783, 1964.

2. S. R. Lederhandler and J. J. Giacoletto, "Measurements of minority carrier lifetime and surface effects in junction devices", Proc. IRE, vol. 43, pp. 447-483, Apr. 1955.

3. R. H. Kingston, "Switching time in junction diodes and transistors," Proc. IRE, vol. 42, pp. 829-834, May 1954.

4. A. Neugroschel, P.J. Chen, S. C. Pao, and F. A. Lindholm, "Diffusion length and lifetime determination in p-n junction solar cells and diodes by forward biased capacitance measurements," IEEE Trans. Electron Devices, vol. ED-25, pp. 485-490, April 1978.

5. A. Neugroschel, "Determination of lifetime and recombination currents in p-n junction solar cells, diodes, and transistors," IEEE Trans. Electron Devices, vol. ED-28, pp. 108-115, Jan. 1981.

6. J. E. Mahan and D. L. Barns, "Depletion layer effects in the open circuit voltage decay lifetime measurements," Solid-State Electronics, vol. 24, pp. 989-994, 1981.

APPENDIX A

Although there are several ways to treat the sudden application of a short circuit replacing forward bias V, perhaps the simplest is to think of voltage -V being applied in series with V at t=0. This treatment emphasizes the change in voltage that starts the ensuing transient. See Fig. A-1(a), below.

Thus at t = 0, this change in voltage raises the right ohmic contact by magnitude eV relative to the left ohmic contact because the ohmic contacts are in equilibrium with the adjoining semiconductor in the sense that the distance between the quasi-Fermi level of majority carriers and the majority-carrier band edge remains the same as in equilibrium. They are in non-equilibrium in the sense that charge carriers can pass through the contacts. At $t = 0^+$, some arbitrarily small time after the application of the short circuit, the change in applied voltage has caused electrons to exit the n-type material adjacent to the contact, leaving behind unbared donor atoms and the positive charge shown in Fig. A-1(b). Similarly holes exit the p-type material (electrons enter the valence band from the metal), giving rise to the negative charge shown in Fig. A.1(b). A near delta function of current i(t), flowing in the direction shown in Fig. A.1(a), establishes this charge configuration at $t = 0^+$. Note that i(t) during the entire transient for $t > 0$ flows in a direction opposite to that occuring for negative time because the transient results in removing the electrons and hole present under forward V.

Having established the existence of this negative charge, we now consider what happens subsequently. Here enters a result developed earlier from operating on Maxwell's equation by the divergence operator:

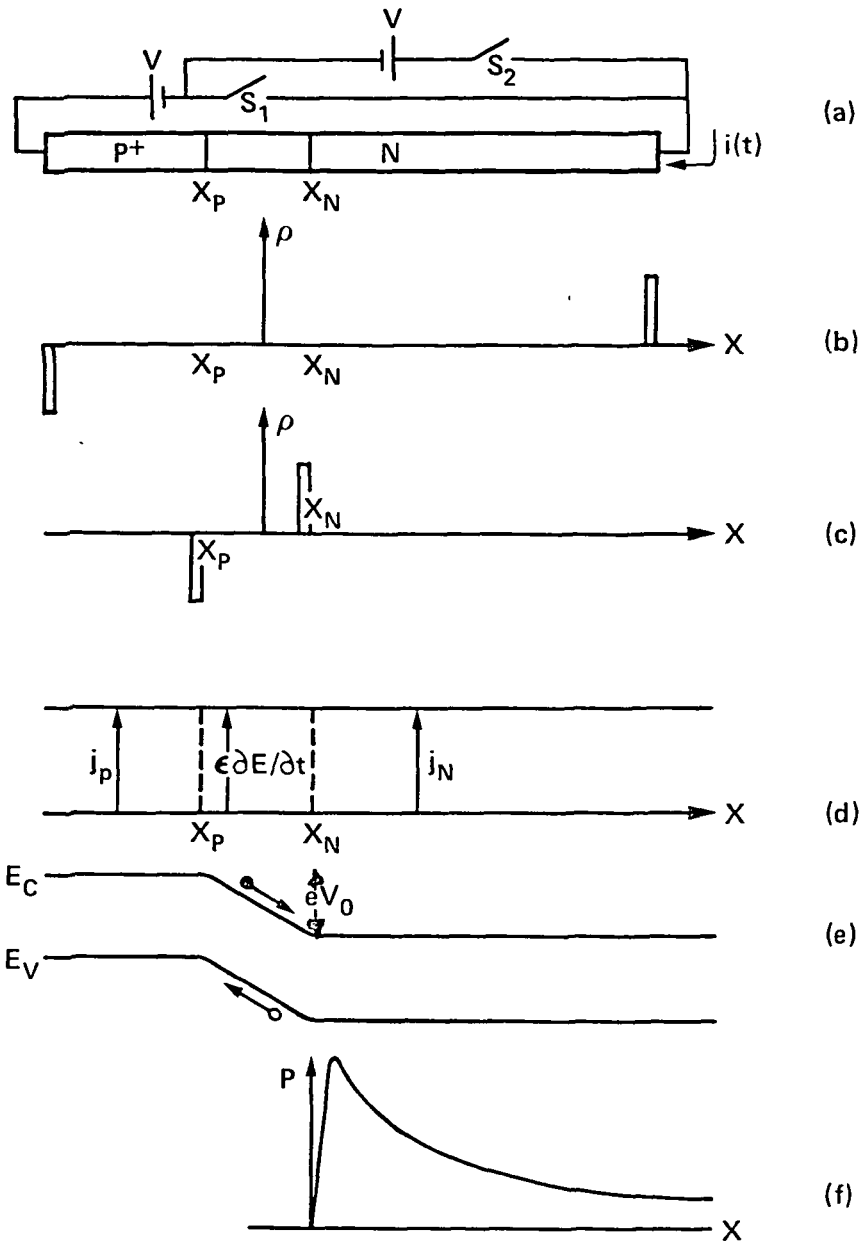

Figure A-1

(a) For $t < 0$, switch S_1 is closed, S_2 is open; conversely for $t > 0$; the junction space-charge region is defined by $x_p < x < x_N$. (b) charge density at $t = 0^+$. (c) charge density for t of the order of a dielectric relaxation time. (d) the total current is x-independent but is essentially majority-carrier convection current in the two quasi-neutral regions and is displacement current in the space-charge region for t of the order of a dielectric relaxation time. (e) electrons and holes drift out of the space-charge region in a transit time. (f) the resulting excess hole density in the space-charge region after a transit time has lapsed.

$$0 = \text{div curl } H = \text{div } j_N + \text{div } j_p + \text{div}[\partial(\varepsilon E)/\partial t] \quad . \qquad (A.1)$$

From this result, two consequences emerge: (1) the charges in Fig. A-1(b) redistribute to the positions shown in Fig. A-1(c) within the order of a dielectric relaxation time $\tau = \varepsilon/\sigma$; and (2) the total current is solenoidal, that is, its divergence is zero, where here the total current includes the displacement current.

The consequence of (2) is illustrated in Fig. A-1(d) for a particular time of order of τ. Notice the large time-rate of change of electric field E within the junction space-charge region, $x_p < x < x_N$. Here we have employed a one-dimensional model so that the operator div becomes the operator $\partial/\partial x$. Thus we see that the electric field in the space charge region grows rapidly so that within t of the order of τ the barrier height has returned to its near equilibrium value and the electric field is several times larger than it was in negative time. But in negative time, the drift and diffusion tendencies of the junction space-charge region were perturbed only by perhaps one part in 10^4 in the forward voltage steady state; that is, the space-charge region was in quasi-equilibrium. For t of the order of τ, the drift tendency now overwhelms the diffusion tendency, and holes and electrons drift out of the space charge region in a transit time τ' determined by $x_N - x_p$/velocity where the velocity approaches the scatter limited velocity because of the high field (Fig. A-1(e)). For typical devices, τ' will be of the order of 10^{-11} s. After this time has passed, the hole and electron concentrations will have returned nearly to their equilibrium values.

Because 10^{-11} s is a time not observed by typical measurement equipment, we think of the initial condition established by shorting the terminals suddenly as that of quasi-neutral regions still storing approximately the same excess charge as was present in the steady state of negative time, of a space-charge region at the equilibrium barrier height and devoid of excess holes and electrons, and as an excess minority carrier density in the quasi-neutral regions that drops sharply to zero at the space-charge region edges (Fig. A-1(f)).

APPENDIX B

Determination of the Eigenvalues for SCCD and OCVD

In this report, we have two Eigenvalue equations, Eqs. (9) and (11), that determine s_i of each mode for OCVD and SCCD. These are

$$\coth(X_{QNB}(1 + s_i \tau_p)^{1/2}/L_p) + D_p(1 + s_i \tau_p)/L_p S_{eff} = 0 \qquad (9)$$

and

$$1 + (D_p(1 + s_i \tau_p)^{1/2}/L_p S_{eff})\coth(X_{QNB}(1 + s_i \tau_p)^{1/2}/L_p) = 0 \quad . \qquad (10)$$

In (9) and (11), Eigenvalues exist only if

$$1 + s_i \tau_p \leq 0 \ (\text{or } s_i \leq -1/\tau_p \text{ or } \tau_i > \tau_p) \qquad (B\text{-}1)$$

where $\tau_i = -1/s_i$.

Granting (B-1), we have

$$(1 + s_i \tau_p)^{1/2} = j(-1\text{-}s_i \tau_p)^{1/2} \quad ,$$

where $(-1\text{-}s_i \tau_p) \geq 0$. Replacing $(1 + s_i \tau_p)^{1/2}$ in (9) and (11) with $j(-1\text{-}s_i \tau_p)^{1/2}$ yields

$$\cot(X_{QNB}K_i/L_p) - (D_p K_i/L_p) = 0 \qquad (B\text{-}2)$$

and

$$1 + (D_p K_i / L_p S_{eff}) \cot(X_{QNB} K_i / L_p) = 0 \quad , \tag{B-3}$$

where

$$K_i = (-1 - s_i \tau_p)^{1/2} \quad .$$

Eqs. (9) and (B-2) are identical and so are (11) and (B-3) under the condition of (B-1). (B-2) and (B-3) imply an infinite number of Eigenvalues as shown in Figs. B-1 and B-2.

For SSCD the vanishing determinant of the inverse of matrix A of Eq. (6) provides an alternate method for determining the Eigenvalues s_i, but no such systematic method exists for OCVD. More details regarding this are planned for future publications.

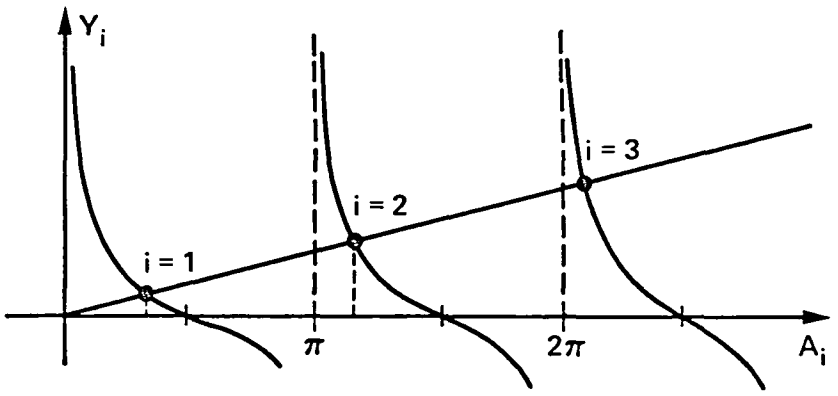

Fig. B-1 The eigenvalues for OCVD where $Y_i = \cot(A_i)$, $A_i = X_{QNB}K_i/L_P$ and $Y_i = (D_P S_{EFF}/X_{QNB})A_i$

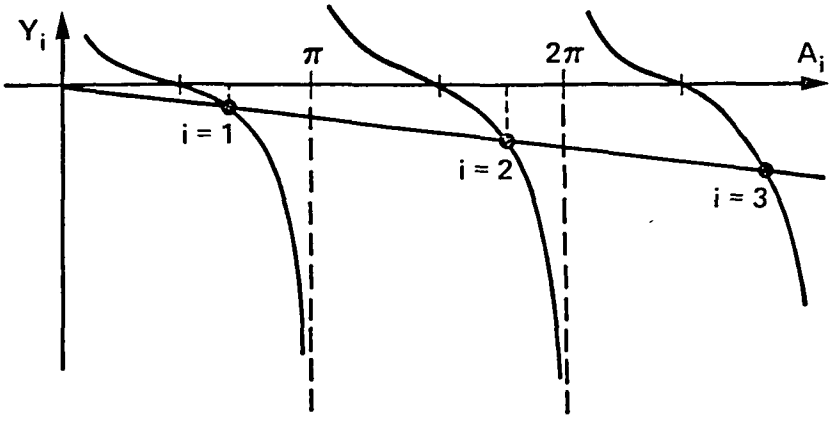

Fig. B-2 The eigenvalues for SCCD where $Y_i = \cot A_i$, $A_i = X_{QNB}K_i/L_P$ and $Y_i = -(X_{QNB}/D_P S_{EFF})A_i$